

SPATIAL TRANSCRIPTOMIC ASSESSMENTS OF GENE EXPRESSION PROFILES IN HUMAN PERI-IMPLANT LESIONS.

Dionigi C.¹, Larsson L.¹ & Berglundh T.^{1,2}

1. Department of Periodontology, Institute of Odontology, The Sahlgrenska Academy at University of Gothenburg, Gothenburg, Sweden.
2. Clinic of Periodontics, Public Dental Service, Region Västra Götaland, Gothenburg, Sweden.

SIoP – Premio H.M. Goldman 2024 – lavoro vincitore sessione RICERCA

In manuscript.

Abstract

Aim: To analyze gene expression profiles in human tissue samples obtained from dental implant sites with or without peri-implantitis.

M&M: Soft tissue biopsies obtained from patients presenting with ≥ 1 implants with severe peri-implantitis, and ≥ 1 adjacent reference implants with either healthy peri-implant tissues or peri-implant mucositis were analyzed by spatial transcriptomics and RNA-sequencing.

Results: Spatial transcriptomics revealed a clear association between 12 distinct gene clusters and specific tissue compartments in both groups of specimens. The strongest gene activity was found in epithelial and infiltrated connective tissue areas and peri-implantitis sites showed higher levels of gene activity compared to samples from reference sites. Among the most significantly differentially expressed genes, CXCL13 and CXCL5 were two of the most up-regulated ones. Numerous keratin-encoding genes were down-regulated in peri-implantitis lesions when compared to reference implant sites. Pathways related to “B cell receptor signaling”, “response to LPS”, and “neutrophil chemotaxis” were up-regulated in peri-implantitis specimens compared to reference sites. On the contrary, pathways connected to “wound healing”, “antimicrobial humoral response”, and “extracellular matrix organization were down-regulated.

Conclusions: Several biological pathways specific for the activation of the host response towards bacterial insults were clearly dysregulated in peri-implantitis when compared to reference implant sites.

Introduction

Along with the increase of the prevalence of individuals treated with dental implants in the last 10 years, peri-implant diseases have become a major and growing problem in dentistry. If left untreated, peri-implantitis can result in implant loss and thereby compromise the stability of the implant-supported prostheses and the overall oral function. The consequences may lead to discomfort and a significant economic and resource burden for the patient (Karlsson et al. 2022). Thus, investigations aiming at unravelling the functional characteristics of the peri-implantitis lesion will provide further understanding of the prevention and management of the disease.

The majority of studies analyzing human biopsies obtained from peri-implantitis lesions relied on immunohistochemical methods. Overall, such findings revealed that peri-implantitis lesions were characterized by large inflammatory cell infiltrates with high densities of plasma cells, B-cells and neutrophils (Gualini & Berglundh, 2003; Berglundh et al., 2004; Carcuac & Berglundh, 2014; Galindo-Moreno et al., 2017). In addition, the cellular infiltrate displayed a gradient-like distribution with higher densities of cells towards the pocket epithelium, thereby illustrating an exacerbated host response in the proximity to the bacterial insult (Dionigi et al., 2020). Despite the comprehensive data on phenotype markers and relevant inflammatory mediators in the targeted tissues obtained in the immunohistochemical analyses, the results were limited to the preselected set of antibodies that was used.

Reports on gene expression profiles in human peri-implantitis tissues identified several biological pathways associated with the activation of the host response (Duarte et al., 2009; Becker et al., 2012; Mardegan et al., 2017; Figueiredo et al., 2020; Giro et al., 2021; Martin et al., 2021; Kheder et al., 2023). Notably, RNA/DNA amplification techniques (e.g., RT-qPCR), microarray methods and next-generation sequencing techniques (e.g., RNA-sequencing) commonly involve tissue homogenization as a step in the sample preparation for gene expression analysis. Homogenization is necessary to disrupt tissue structures and release cellular contents, thereby making RNA or DNA accessible for further analysis. The processing of tissue sample, however, results in a complete loss of the spatial information of gene expression within tissues.

The recently introduced “spatial transcriptomic” technique (Stahl et al., 2016), appointed as “method of the year” in 2020 (Marx, 2021), allows high-throughput gene expression analysis and large-scale data visualization onto corresponding intact tissue sections, almost at the single-cell level. As the spatial context is crucial for understanding tissue function and disease processes, this technique bridges the gap between molecular biology and spatial tissue organization (Asp et al., 2020).

Thus, the aim of the present study was to detect differences in gene expression profiles in human tissue samples obtained from dental implant sites with or without peri-implantitis using a novel approach integrating spatial transcriptomic and RNA-sequencing techniques.

Material & Methods

Study population

Ten patients scheduled for the surgical treatment of peri-implantitis-affected dental implants were consecutively recruited from the Specialist Clinic of Periodontics in Gothenburg, Public Dental Services, Region Västra Götaland, Sweden. The study protocol was approved by the Swedish Ethical Review Authority (Dnr 2021- 00508). To be included in the study, patients had to present with ≥ 1 implants with severe peri- implantitis, and

≥ 1 adjacent reference implants with either healthy peri-implant tissues or peri-implant mucositis. Peri-implantitis was defined as peri-implant probing pocket depth (PPD) of ≥ 7 mm, bleeding and/or suppuration on probing (BoP/SoP) and radiographically confirmed bone levels of ≥ 3 mm. Peri-implant mucositis was distinguished from peri-implantitis by PPD ≤ 5 mm and bone levels of < 3 mm.

Exclusion criteria comprised: patients that received previous peri-implant surgical interventions at diseased implant sites, use of systemic/local antibiotics in the last 6 months and presence of systemic conditions affecting peri-implant tissues and/or impeding the surgical intervention (e.g., uncontrolled diabetes,

immunosuppressive medication). Patients were excluded if peri-implantitis and reference implant sites differed in terms of time of implant installation and/or implant system.

Before enrolment, the study design and purpose were explained in detail to all subjects. Upon acceptance, patients signed an informed consent. Oral hygiene instructions and a professional supra-gingival cleaning session were given to all patients before the surgical treatment. Details on patient characteristics and clinical measures obtained prior to the surgical interventions are summarized in [Supplementary Table 1](#) and [Supplementary Table 2](#).

Biopsy retrieval

Following local anesthesia, biopsies were dissected prior to flap elevation following two parallel incisions (3-5 mm apart) extending from the soft tissue margin to the bone crest from peri-implantitis and reference implant sites. A perpendicular incision was placed at a distance of about 4-5 mm from the implant body. After dissection, the biopsies were copiously rinsed with saline, mounted in plastic cassettes (Tissue-Tek Paraform Sectionable Cassette System; Sakura Finetek Europe, Netherlands) and placed in 4% buffered formalin for 48 hours. Samples were stored in 70% ethanol, kept at 4°C, subsequently dehydrated in increasing grades of ethanol and embedded in paraffin until further processing (Formalin-Fixed Paraffin-Embedded; “FFPE samples”).

After flap elevation, at the same “FFPE sample” collection sites, a small additional peri-implant connective tissue portion (about 1-2 mm³) was dissected both at peri-implantitis and reference implants. Samples were rinsed with saline, placed in Eppendorf tubes, immersed in RNAlater (AMBION, Inc., Austin, Texas, USA) at 4°C for 48 hours and stored at -80°C until further processing (“RNA-seq samples”).

Spatial transcriptomics

Five-mm-thick sections were produced in a microtome from 4 “FFPE samples” (2 paired samples obtained in 2 patients) and prepared according to the Visium CytAssist Spatial Gene Expression for FFPE-Tissue

Preparation Guide (CG000518, 10× Genomics, Pleasanton, CA, USA) in collaboration with the SciLife Laboratory (National Genomics Infrastructure, Karolinska Institute and Stockholm University, Sweden). The four samples presented with DV200 values $\geq 70\%$ and, hence, fulfilled criteria for further processing and analysis.

Sections were mounted on standard glass slides, dewaxed, stained with hematoxylin & eosin and imaged with a V200 Slide Scanner Olympus Microscope (Evident, Japan). Decrosslinking and tissue permeabilization were performed with a thermocycler at 95°C for 1 hour. Visium CytAssist Spatial Gene Expression v2 slides (6.5mm) were loaded into the Visium CytAssist instrument and placed into close proximity to the glass slides holding the tissue sections. Reverse transcription was performed *in situ* with the probes attached on the Visium CytAssist slides functioning as primers, resulting in complementary DNA (cDNA) coupled to the barcoded probes on the array. The tissue samples were enzymatically digested with the CytAssist Enabled RNA Digestion & Tissue Removal and removed from the glass slides. The probes on the Visium CytAssist slide were cleaved and the barcoded cDNA was collected. Libraries were generated and sequenced.

The final libraries comprised standard Illumina paired-end constructs. Once quantified and normalized,

the libraries were denatured and diluted, as recommended for Illumina sequencing platforms. All samples were sequenced on NovaSeq6000 (NovaSeq Control Software 1.8.0/RTA v3.4.4) with a 151nt(Read1)-19nt(Index1)-10nt(Index2)-151nt(Read2) setup using 'NovaSeqXp' workflow in 'S4' mode flowcell. Raw sequencing data were demultiplexed and converted to FastQ. The Bcl to FastQ conversion was performed using bcl2fastq_v2.20.0.422 from the CASAVA software suite. The quality scale used was Sanger / phred33 / Illumina 1.8+. Standardized bioinformatics quality control checks were performed including yield, sequence read quality and cross-sample contamination checking (ISO/IEC 17025). Libraries were sequenced with depths ≥ 114 Mreads/sample [114.24-167.74] and presented with a $\geq 87\%$ aggregated percentage of bases quality score >30 . Image alignment, demultiplexing on spatial barcodes and basic Visium quality checks were performed using Space Ranger and Loupe Browser (10xGenomics).

Data analysis was performed in collaboration with the CORE Facility – Bioinformatics of the Sahlgrenska Academy, University of Gothenburg, Sweden. Filtered gene spot matrix and high-resolution fiducial aligned images were used for downstream data analysis in Seurat (version 4.9.9.9045). Each sample was filtered according to the following protocol: cells were filtered if the percentage of mitochondrial genes was higher than 20% and if the number of unique molecular identifier (UMI) counts per spot was less than 130. Samples were individually normalized and variance-stabilized using regularized negative binomial regression with the R package SCTransform (version 0.3.5) where the percentage of mitochondrial expression was regressed out and the number of variable genes was set to 6000 out of 18000 total available genes. The number of variable genes was further used to create anchors for integration between samples in order to reduce batch affect and resolve for possible differences in sample tissue quality. Then PCA $n_pcs=10$, FindNeighbors, Clustering with resolution set to 0.6 and UMAP dimensionality reduction using 10 dimensions were used to identify 12 stable clusters across peri- implantitis and reference implant samples. Identifying differentially expressed markers for disease-specific clusters compared to reference was done using the 'FindMarker' function from Seurat. Genes were considered differentially expressed with adjusted p values <0.05 . Log-fold change was used to identify the magnitude of change in gene expression between groups. Threshold levels of $\text{Log}_2\text{FC} \geq 2$ and $\text{Log}_2\text{FC} \leq -2$ were applied to identify the most significantly differentially expressed genes.

RNA-sequencing

The “RNA-seq” samples ($n=20$, 10 pairs) were treated with the RNeasy Plus Micro Kit (Quiagen, Germany) for the extraction of total RNA following the manufacturer's instructions. The extracted total RNA content was eluted in 14 μl of RNase-free water and stored at -80°C . Total RNA integrity and size distribution were checked with the Agilent Tapestation 4200 system. All samples passed the quality check with optimized concentrations of total RNA [range 34-463 $\text{ng}/\mu\text{L}$] and RIN scores ≥ 5 [range 5-9].

The “Illumina Stranded mRNA Prep Ligation” protocol was used for library preparation by experts from the CORE Facility – Genomics of the Sahlgrenska Academy at University of Gothenburg, Sweden. After 11 PCR cycles and purification of the adapter-ligated fragments with magnetic beads, the libraries were normalized down to 1 nM, pooled together, diluted to 0.5 nM and standard run on a S2 flowcell on the NovaSeq 6000 (Illumina). Libraries were sequenced with an average depth of approximately 59.3 (± 11.4) Mreads/sample.

Data analysis was performed in collaboration with the CORE Facility – Bioinformatics of the Sahlgrenska Academy, University of Gothenburg, Sweden. First, the quality of the reads was examined using

fastqc/0.11.9 (Andrews S., 2010) and the resulting quality reports were summarized using MultiQC/1.9 (Etwels et al., 2016). The reads were quality filtered using Trim Galore/0.4.0 (Krueger et al., 2021) while adapters were removed using Cutadapt/1.9 (Martin M., 2011). The quality-filtered reads were aligned towards the human reference genome GRCh38.109 using STAR/2.7.10b (Dobin et al., 2012). Infer experiment within RSeQC/5.0.1 (Wang et al., 2012) was used to evaluate the strandness of the data. Featurecounts within the subread/2.0.4 package (Liao et al., 2014) was used to gather the gene counts. The differential expression analysis was run in the R/4.1.3 package (R Core Team, 2022) DESeq2/1.34.0 (Love et al., 2014). Genes were considered differentially expressed with adjusted p values <0.05 . Log-fold change was used to identify the magnitude of change in gene expression between groups. Threshold levels of $\text{Log}_2\text{FC} \geq 1$ and $\text{Log}_2\text{FC} \leq -1$ were applied to identify the most significantly differentially expressed genes. The package pheatmap/1.0.12 (Kolde et al., 2019) was used to generate the heatmaps. ClusterProfiler/4.2.2 (Wu et al., 2021) was used to perform the overrepresentation analysis for Gene Ontology (Ashburner et al., 2011) and Reactome (Jassal et al., 2020).

Results

Spatial transcriptomics

In total, the spatial transcriptomic analysis identified 4298 differentially expressed genes (DEGs) when looking at the entire SCTransformed dataset in Seurat (adjusted p values <0.05) comparing peri-implantitis versus reference implant sections. Among those, 3949 genes were down-regulated, and 349 genes were up-regulated.

Results on the amounts of transcripts detected in each spot and their localization within the two pairs of tissue samples are presented in [Fig. 1](#). It was demonstrated that the oral and the pocket epithelium as well as the infiltrated connective tissue (ICT) areas in both peri-implantitis and reference implant sites presented with the highest gene activity in comparison to non-infiltrated connective tissue (NCT) portions. In addition, peri-implantitis sites showed overall higher degrees of gene activity when compared to reference implant sites.

The “Uniform manifold approximation and projection” (UMAP) dimensionality reduction technique was used to visualize and analyze high-dimensional spatial transcriptomic data in a two-dimensional space. Twelve distinct clusters of gene expression signatures were identified, and results are illustrated in [Fig. 2a](#) and [Fig. 2b](#). The UMAP visualization revealed stronger gene expression patterns in peri-implantitis sites for all clusters except for cluster 9.

The identified clusters were color-coded and visualized according to their spatial coordinates onto the hematoxylin & eosin-stained images, as represented in [Fig. 3a](#) and [Fig. 3b](#). A clear association was observed between clusters and specific regions in the samples in both groups. Thus, clusters 2, 5, 7 and 12 were distinctly located within the ICT compartment and clusters 6, 8, 10 and 11 matched epithelial tissues. While clusters 0 and 9 were confined to the NCT area, no specific tissue areas were identified for clusters 1, 3 and 4.

The differential gene expression analysis of the 4 clusters specific for the ICT areas revealed 188 up-regulated and 1247 down-regulated genes in peri-implantitis specimens versus samples from reference implant sites. The 12 most highly up- and the 31 most highly down-regulated genes observed in the ICT clusters (after filtering with a threshold Log_2 fold change ≥ 2 or ≤ -2) are reported in [Table 1](#). One up-regulated and 9 down-regulated genes, highlighted in red color in the table, were consistently expressed among the 4 clusters. The spatial distribution of the most highly up-regulated genes in peri-implantitis tissues is visualized in [Fig. 4](#).

Gene ontology (GO) enrichment analysis was performed to explore the biological processes involved in each of the 4 clusters that were specific for the ICT compartment ([Supplementary Fig. 1a](#) and [Supplementary Fig. 1b](#)). Pathways related to “B cell receptor signaling”, “epidermal cell differentiation”, “response to LPS”, “humoral immune response” and “neutrophil chemotaxis” were all found to be up-regulated in peri-implantitis specimens compared to reference implant sites. On the contrary, pathways connected to “wound healing”, “antimicrobial humoral response”, “regulation of angiogenesis”, “extracellular matrix organization”, “connective tissue development”, “collagen fibril organization” and “regulation of epithelial/endothelial cell apoptotic process” were downregulated.

RNA-sequencing

The RNA-sequencing analysis revealed 2878 significantly up- and 2263 down-regulated genes (adjusted p values <0.05) in peri-implantitis versus reference implant samples. The 20 most highly up- and down-regulated genes are reported in Table 2. The hierarchical clustering of the 20 genes (reported with EnsemblID) with the strongest gene-expression levels (Log_2 fold change) are shown in the heatmap in Fig. 5a. The volcano plot in Fig. 5b illustrates the significantly (adjusted p values <0.05) up- and down-regulated genes (red color) after filtering application ($\text{Log}_2\text{FC} \geq 1$ or ≤ -1).

Gene ontology (GO) and Reactome enrichment analyses were performed to explore biological functions (Supplementary Fig. 2). The most up-regulated GO functions in peri-implantitis samples were associated with the “immune response regulating-signaling”, “histone modification” and “activation of immune response” pathways when compared to reference implant samples. The most up-regulated Reactome pathways in peri-implantitis samples were connected to the “RHO GTPase cycle”, the “neutrophil degranulation” and the “extracellular matrix organization” pathways.

Discussion

The present study evaluated differences in gene expression profiles in human tissue samples obtained from peri-implantitis and reference implant sites by integrating spatial transcriptomic and RNA-sequencing data. The analysis revealed clear associations between distinct gene clusters and specific tissue compartments in both groups of specimens. In addition, peri-implantitis sites showed higher levels of gene activity compared to samples from reference implant sites. Gene-set enrichment analysis revealed that several important biological pathways (e.g., “regulation of antimicrobial host response”, “collagen fibril organization” and “regulation of angiogenesis”) were severely dysregulated in peri-implantitis lesions when compared to reference implant sites.

The strategy of using paired specimens representing destructive and non-destructive peri-implant lesions from the same patients in the present study effectively reduced biological variability and technical variation among samples. As a result, we identified twelve distinct clusters of gene expression signatures and a strong association between clusters and tissue-specific areas was observed. A similar approach was employed by a recent study that compared soft tissue samples obtained from peri-implantitis, periodontitis and healthy gingival tissues by using RNA-sequencing and RT-qPCR (Oh et al. 2023).

By superimposing the gene clusters distribution on matching histological sections, our analysis revealed that the position of 4 distinct gene clusters coincided with the infiltrated connective tissue (ICT) compartment. Additional filtering procedures resulted in the detection of 13 up-regulated and 31 down-regulated genes in the ICT of peri-implantitis when compared with the ICT of reference implant sites. Furthermore, the Gene Ontology and Reactome enrichment analyses showed that the up-regulated genes were associated with several biological pathways specific for the activation of the host response towards bacterial insults.

Interestingly, two of the most up-regulated genes in the present study were the C-X-C motif chemokine ligand 13 (CXCL13; found in cluster 5 from spatial transcriptomic results) and the C-X-C motif chemokine ligand 5 (CXCL5; from RNA-seq results). While CXCL13 is also known as “B lymphocyte chemoattractant” and plays a role in B cell activation and organization (Nakajima et al., 2008), CXCL5 participates in the regulation of neutrophil chemotaxis and in the activation of angiogenesis processes and is also known as

“epithelial-derived neutrophil-activating peptide 78” (Barros & Offenbacher, 2014). In a study on gene expression profiles using RNA-sequencing and gene-set enrichment analysis, Kheder et al., (2023) reported that genes encoding for IL1B, CDK3, IL27 and CD86 were up-regulated in sites with severe peri-implantitis (termed “failed implants”) as opposed to healthy gingival tissues at teeth. The validity of the results presented in the study by Kheder et al. (2023) in regard to data reported in the current investigation is unclear, as no comparisons were made on gene expression profiles between peri-implantitis and reference implant sites.

Several of the observed down-regulated pathways in the current study were associated with keratin genes. While the underlying mechanisms behind this observation are not fully understood, findings made in pre-clinical studies and in analysis of human biopsy material need to be considered. One of the main characteristics of peri-implantitis lesions, which also is a distinct difference to periodontitis lesions around teeth, is the lack of an epithelial lining in the apical part of the tissue in the pocket area facing the implant. Consequently, the apical portion of the peri-implantitis lesion is left uncovered and in direct contact with the bacterial biofilm residing on the implant surface (Lindhe et al., 1992; Carcuac et al., 2013, Carcuac & Berglundh 2014). In addition, while keratin genes are primarily expressed by epithelial cells, other cells, e.g., immune cells, fibroblasts, and endothelial cells, may also express keratin genes as a host defense mechanism in inflammation (Traweek et al., 1993; Katagata et al. 2002). The findings of the present study corroborate this concept, as several pathways related to “wound healing”, “regulation of angiogenesis”, “extra-cellular matrix organization” and “collagen fibril organization” were down-regulated in peri-implantitis sites when compared with reference implant specimens.

The spatial transcriptomic analysis in the present study also revealed that the strongest gene activity was found in epithelial and infiltrated connective tissue areas. This finding is explained by the higher cellular densities in epithelial and infiltrated connective tissue areas than in non-infiltrated connective tissue compartments. In addition, inflammation is often associated with an up-regulation of cells of the immune response, which leads to increased expressions of genes related to immune signaling and activation of inflammatory mediators. Similar results were reported by Lundmark et al. (2018) who employed spatial transcriptomics to evaluate gene expression profiles in periodontitis and healthy gingival tissues in humans. The authors reported on higher amounts of transcripts per spot in epithelial and infiltrated connective tissue areas than in connective tissue portions with no signs of inflammatory cell infiltration.

In conclusion, peri-implantitis lesions revealed higher levels of gene activity when compared to reference implant sites. The integration of next-generation sequencing techniques allowed the observation of several dysregulated genes in inflamed diseased sites. The possibility to visualize clusters of gene signatures within tissue sections offered by the spatial transcriptomic method, provided the opportunity to restrict gene expression analysis only to clusters of interest. In addition, the risk for dilution of results was diminished as tissue samples could be analyzed in their entirety without the need for sample homogenization. Similarly, the choice of analyzing with RNA-sequencing tissue portions restricted to the connective tissue directly facing the implants resulted in high levels of agreement with data obtained from spatial transcriptomics. The most obvious drawback of employing such novel techniques in the present study, resided in the substantial investment of both financial and time resources. This is reflected by the limited number of samples that were analyzed in the present study. Further improvement of the new technologies, however, may result in faster processing and diminished costs.

References

- Andrews S. FastQC: A quality Control Tool for high throughput sequence data. Published online June 2010. <https://qubeshub.org/resources/fastqc>
- Aran D, Looney AP, Liu L et al. (2019). Reference-based analysis of lung single-cell sequencing reveals a transitional profibrotic macrophage. *Nat. Immunol.* 20, 163–172.
- Ashburner M, Ball CA, Blake JA, et al. The Gene Ontology Consortium. Gene ontology: tool for the unification of biology. *Nat Genet.* 2011;25(1):25-29. doi:10.1038/75556
- Asp M, Bergenstråhle J, Lundeberg J. Spatially Resolved Transcriptomes-Next Generation Tools for Tissue Exploration. *Bioessays.* 2020 Oct;42(10):e1900221. doi: 10.1002/bies.201900221. Epub 2020 May 4. PMID: 32363691.
- Barros, S. P., & Offenbacher, S. (2014). Modifiable risk factors in periodontal disease: epigenetic regulation of gene expression in the inflammatory response. *Periodontol 2000*, 64(1), 95-110. doi:10.1111/prd.12000.
- Becker, S. T., Beck-Broichsitter, B. E., Graetz, C., Dörfer, C. E., Wiltfang, J., & Häsler, R. (2014). Peri-implantitis versus periodontitis: Functional differences indicated by transcriptome profiling. *Clinical Implant Dentistry and Related Research*, 16(3), 401-411.
- Carcuac O, Berglundh T. Composition of human peri-implantitis and periodontitis lesions. *J Dent Res.* 2014 Nov;93(11):1083-8. doi: 10.1177/0022034514551754. Epub 2014 Sep 26. PMID: 25261052; PMCID: PMC4293768.
- Carcuac, O., Abrahamsson, I., Albouy, J. P., Linder, E., Larsson, L., & Berglundh, T. (2013). Experimental periodontitis and peri-implantitis in dogs. *Clinical Oral Implants Research*, 24(4), 363-371.
- Dionigi C, Larsson L, Carcuac O, Berglundh T. Cellular expression of DNA damage/repair and reactive oxygen/nitrogen species in human periodontitis and peri-implantitis lesions. *J Clin Periodontol.* 2020 Dec;47(12):1466-1475. doi: 10.1111/jcpe.13370. Epub 2020 Nov 9. PMID: 32996143; PMCID: PMC7756411.
- Dobin A, Davis CA, Schlesinger F, et al. STAR: ultrafast universal RNA-seq aligner. *Bioinformatics.* 2012;29(1):15-21. doi:10.1093/bioinformatics/bts635.
- Duarte PM, de Mendonça AC, Máximo MB, Santos VR, Bastos MF, Nociti Júnior FH. Differential cytokine expressions affect the severity of peri-implant disease. *Clin Oral Implants Res.* 2009 May;20(5):514-20. doi: 10.1111/j.1600-0501.2008.01680.x. Epub 2009 Mar 11. PMID: 19302394.
- Ewels P, Magnusson M, Lundin S, Käller M. MultiQC: Summarize analysis results for multiple tools and samples in a single report. *Bioinformatics.* Published online 2016. doi:10.1093/bioinformatics/btw354
- Figueiredo LC, Bueno-Silva B, Nogueira CFP, Valadares LC, Garcia KMM, Filho GCDL, Milanello L, Esteves FM, Shibli JA, Miranda TS. Levels of Gene Expression of Immunological Biomarkers in Peri-Implant and Periodontal Tissues. *Int J Environ Res Public Health.* 2020 Dec 6;17(23):9100. doi: 10.3390/ijerph17239100. PMID: 33291232; PMCID: PMC7730812.
- Galindo-Moreno, P., López-Martínez, J., Caba-Molina, M. et al (2017). Morphological and immunophenotypical differences between chronic periodontitis and peri-implantitis – A cross-sectional study. *European Journal of Oral Implantology*, 10(4), 453-463.
- Giro G, Tebar A, Franco L, Racy D, Bastos MF, Shibli JA. Treg and TH17 link to immune response in individuals with peri-implantitis: a preliminary report. *Clin Oral Investig.* 2021 Mar;25(3):1291-1297. doi: 10.1007/s00784-020-03435-w. Epub 2020 Jun 27. PMID: 32594309.
- Gualini F, Berglundh T. Immunohistochemical characteristics of inflammatory lesions at implants. *J Clin Periodontol.* 2003 Jan;30(1):14-8. doi: 10.1034/j.1600-051x.2003.300103.x. PMID: 12702106.
- Jassal B, Matthews L, Viteri G, et al. The reactome pathway knowledgebase. *Nucleic Acids*

Res.

2020;48(D1):D498-D503. doi:10.1093/nar/gkz1031

- Karlsson K, Derks J, Wennström JL, Petzold M, Berglundh T. Health economic aspects of implant-supported restorative therapy. *Clin Oral Implants Res.* 2022 Feb;33(2):221-230. doi: 10.1111/clr.13885. Epub 2021 Dec 18. PMID: 34888933.
- Katagata Y, Takeda H, Ishizawa T, Hozumi Y, Kondo S. Occurrence and comparison of the expressed keratins in cultured human fibroblasts, endothelial cells and their sarcomas. *J Dermatol Sci.* 2002 Oct;30(1):1-9. doi: 10.1016/s0923-1811(02)00039-7. PMID: 12354414.
- Kheder W, Bouzid A, Venkatachalam T, Talaat IM, Elemam NM, Raju TK, Sheela S, Jayakumar MN, Maghazachi AA, Samsudin AR, Hamoudi R. Titanium Particles Modulate Lymphocyte and Macrophage Polarization in Peri-Implant Gingival Tissues. *Int J Mol Sci.* 2023 Jul 19;24(14):11644. doi: 10.3390/ijms241411644. PMID: 37511404; PMCID: PMC10381089.
- Kolde R. pheatmap: Pretty Heatmaps. Published online 2019. <https://cran.r-project.org/package=pheatmap>
- Krueger Felix, James Frankie, Ewels Phil, Afyounian Ebrahim S-BB. FelixKrueger/TrimGalore. Published online 2021. doi:<https://doi.org/10.5281/zenodo.5127899>
- Liao Y, Smyth GK, Shi W. featureCounts: an efficient general purpose program for assigning sequence reads to genomic features. *Bioinformatics.* 2014;30(7):923-930. doi:10.1093/bioinformatics/btt656
- Lindhe J, Berglundh T, Ericsson I, Liljenberg B, Marinello C. Experimental breakdown of peri-implant and periodontal tissues. A study in the beagle dog. *Clin Oral Implants Res.* 1992 Mar;3(1):9-16. doi: 10.1034/j.1600-0501.1992.030102.x. PMID: 1420727.
- Love MI, Huber W, Anders S. Moderated estimation of fold change and dispersion for RNA-seq data with DESeq2. *Genome Biol.* 2014;15(12):550. doi:10.1186/s13059-014-0550-8
- Lundmark A, Gerasimcik N, Båge T, Jemt A, Mollbrink A, Salmén F, Lundeborg J, Yucel-Lindberg T. Gene expression profiling of periodontitis-affected gingival tissue by spatial transcriptomics. *Sci Rep.* 2018 Jun 19;8(1):9370. doi: 10.1038/s41598-018-27627-3. PMID: 29921943; PMCID: PMC6008462.
- Mabbott NA et al. (2013). An expression atlas of human primary cells: inference of gene function from coexpression networks. *BMC Genomics* 14, Article 632.
- Mardegan GP, Shibli JA, Roth LA, Faveri M, Giro G, Bastos MF. Transforming growth factor- β , interleukin-17, and IL-23 gene expression profiles associated with human peri-implantitis. *Clin Oral Implants Res.* 2017 Jul;28(7): e10-e15. doi: 10.1111/clr.12846. Epub 2016 Apr 7. PMID: 27062688.
- Martin A, Zhou P, Singh BB, Kotsakis GA. Transcriptome-wide Gene Expression Analysis in Peri-implantitis Reveals Candidate Cellular Pathways. *JDR Clin Trans Res.* 2022 Oct;7(4):415-424. doi: 10.1177/23800844211045297. Epub 2021 Sep 28. PMID: 34583558; PMCID: PMC9490470.
- Martin M. Cutadapt removes adapter sequences from high-throughput sequencing reads. *EMBnet.journal.* 2011;17(1):10. doi:10.14806/ej.17.1.200
- Marx, V. Method of the Year: spatially resolved transcriptomics. *Nat Methods* 18, 9–14 (2021).
- Nakajima, T., Amanuma, R., Ueki-Maruyama, K., Oda, T., Honda, T., Ito, H., & Yamazaki, K. (2008). CXCL13 expression and follicular dendritic cells in relation to B-cell infiltration in periodontal disease tissues. *J Periodontal Res*, 43(6), 635-641.
- Oh, J. M., Kim, Y., Son, H., Kim, Y. H., & Kim, H. J. (2023). Comparative transcriptome analysis of periodontitis and peri-implantitis in human subjects. *J Periodontol.*
- R Core Team (2022). R: A language and environment for statistical computing. R Foundation for Statistical Computing, Vienna, Austria. URL <https://www.R-project.org>.
- Schmiedel B et al. (2018). Impact of Genetic Polymorphisms on Human Immune Cell Gene Expression. *Cell* 175, 1701-1715.
- Ståhl PL, Salmén F, Vickovic S, Lundmark A, Navarro JF, Magnusson J, Giacomello S, Asp M, Westholm JO, Huss M, Mollbrink A, Linnarsson S, Codeluppi S, Borg Å, Pontén F, Costea PI, Sahlén P, Mulder J, Bergmann O,

Lundeberg J, Frisén J. Visualization and analysis of gene expression in tissue sections by spatial transcriptomics. *Science*. 2016 Jul 1;353(6294):78-82. doi: 10.1126/science.aaf2403. PMID: 27365449.

- Traweek ST, Liu J, Battifora H. Keratin gene expression in non-epithelial tissues. Detection with polymerase chain reaction. *Am J Pathol*. 1993 Apr;142(4):1111-8. PMID: 7682761; PMCID: PMC1886881.
- Wang L, Wang S, Li W. RSeQC: Quality control of RNA-seq experiments. *Bioinformatics*. Published online 2012. doi:10.1093/bioinformatics/bts356
- Wu T, Hu E, Xu S, et al. clusterProfiler 4.0: A universal enrichment tool for interpreting omics data. *Innovation*. 2021;2(3):100141. doi:10.1016/j.xinn.2021.100141

Premio Goldman Sldp 2024

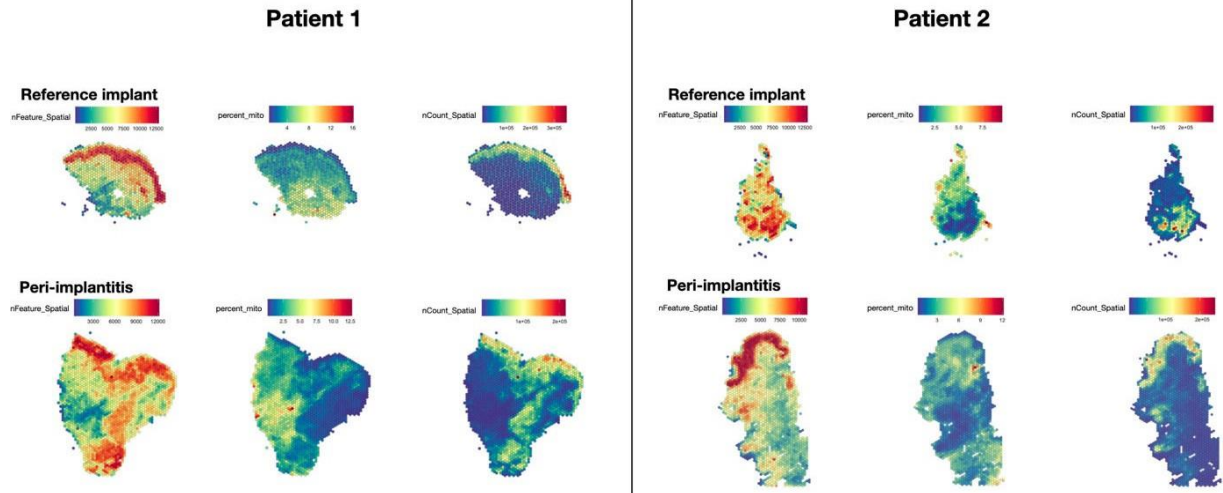


Figure 1. Visualization of gene activity in peri-implantitis and reference implant samples by spatial transcriptomic analysis. The implant-tissue interface is found on the right side in all samples.

Premio Goldman Slap

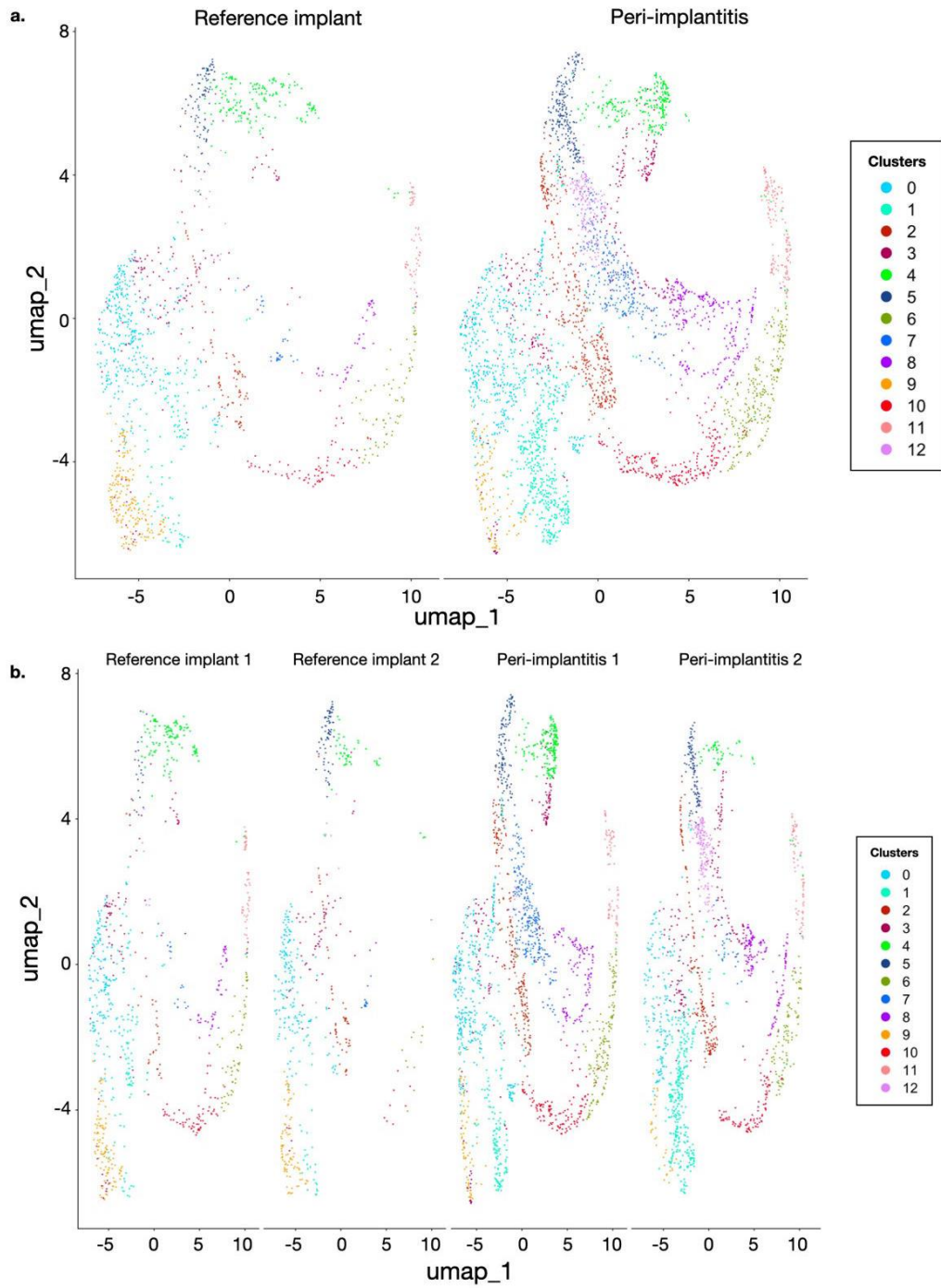


Figure 2. The 12 identified clusters of gene expression profiles found in peri-implantitis and reference implant specimens by spatial transcriptomic analysis. a) Merged data; b) Data in each patient.

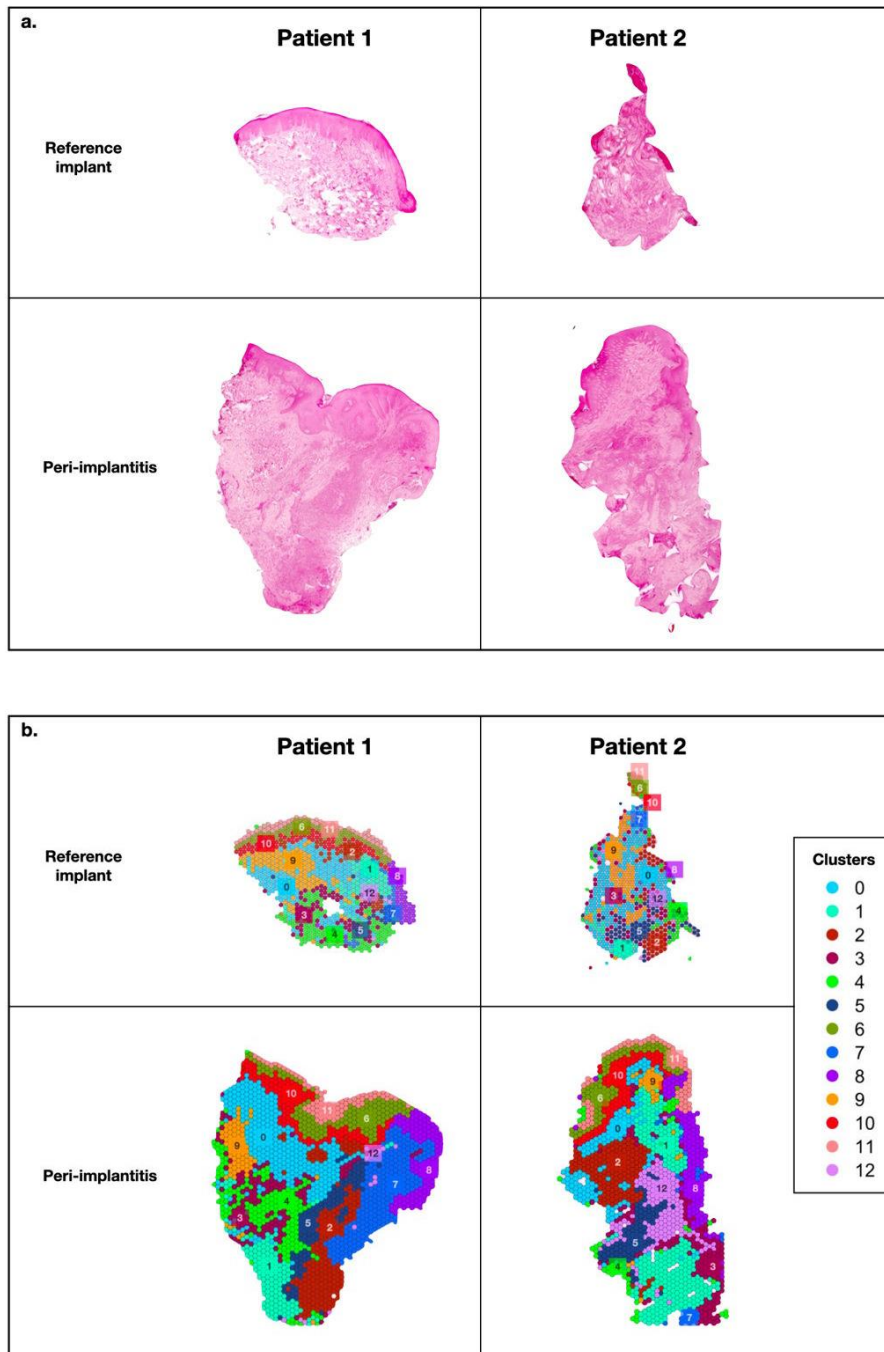


Figure 3.

a) H&E micrographs of peri-implantitis and reference implant specimens. Magnification 5x.

b) Visualization of the 12 distinct clusters of gene expression profiles onto matching H&E sections. The implant-tissue interface is found on the right side in all samples.

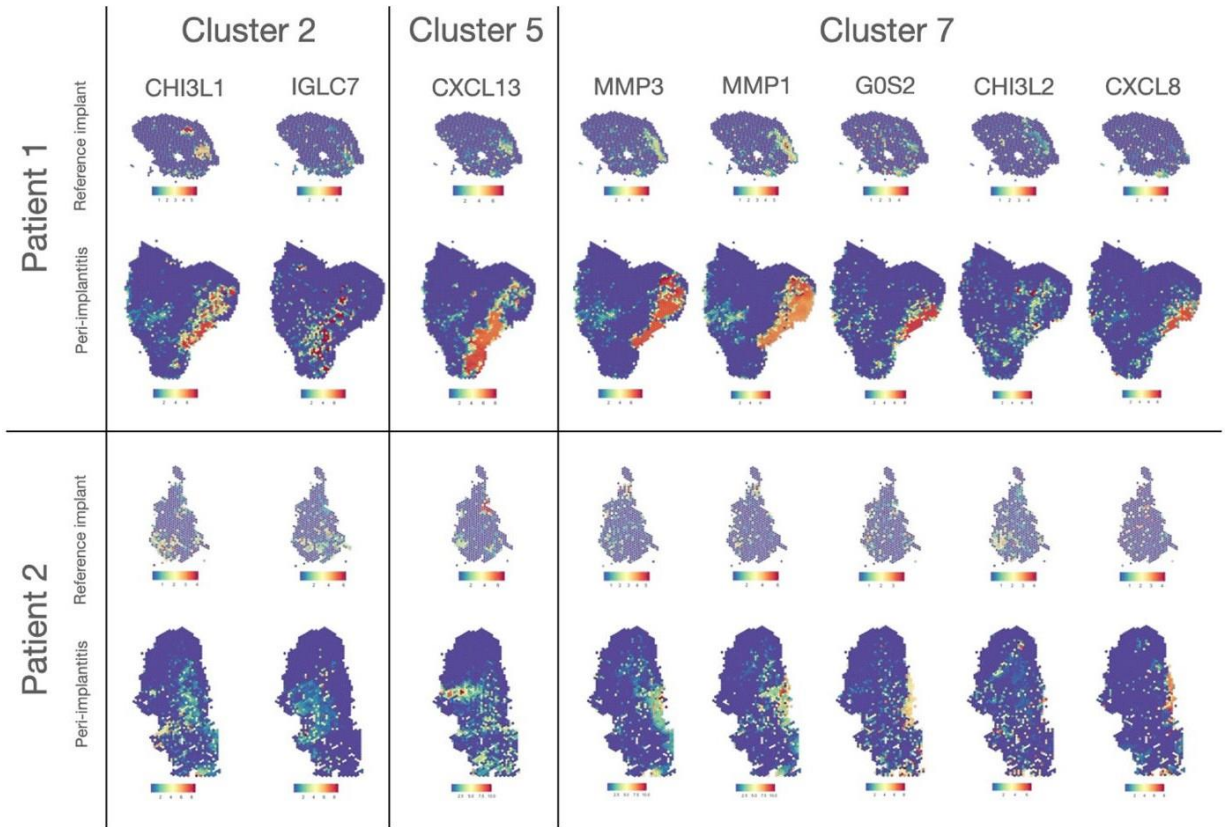


Figure 4. Visualization of the most up-regulated DEGs in clusters 2, 5 and 7 in peri-implantitis and reference implant specimens. The implant-tissue interface is found on the right side in all samples.

Premio Gold

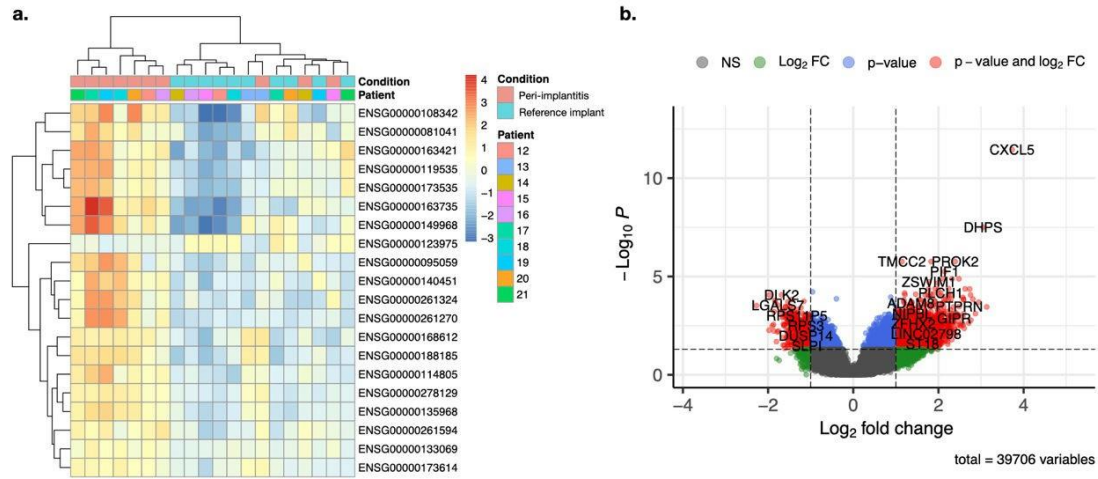


Figure 5. RNA-sequencing results. a) Heatmap showing the hierarchical clustering of the 20 DEGs with strongest gene expression levels (Log_2FC) identified in peri-implantitis versus reference implant specimens. b) Volcano plot illustrating the most up- and down-regulated genes (p adjusted <0.05 and $\text{Log}_2\text{FC} \geq 1$ or ≤ -1).

Table 1 - DEGs identified by spatial transcriptomics in clusters specific for the ICT in peri-implantitis versus reference implant specimens

	Gene symbol	Gene name	Log2 fold change	Adjusted p-value		Gene symbol	Gene name	Log2 fold change	Adjusted p-value	
Cluster 2	Up-regulated genes					Cluster 5	Up-regulated genes			
	CHI3L1	Chitinase-3-like protein 1	2.19	5.53E-07			CXCL13	C-X-C Motif Chemokine Ligand 13	2.21	1.51E-12
	IGLC7	Immunoglobulin lambda constant 7	3.06	0.0326			Down-regulated genes			
	Down-regulated genes						KRT14	Keratin 14	-6.33	0.00271
	KRT13	Keratin 13	-4.97	1.07E-06			KRT16	Keratin 16	-5.41	9.9E-07
	KRT6A	Keratin 6A	-4.93	1.80E-12			KRT5	Keratin 5	-5.03	0.00317
	KRT6B	Keratin 6B	-4.88	1.00E-21			KRT6A	Keratin 6A	-4.93	7.45E-06
	KRT1	Keratin 1	-4.87	7.44E-09			KRT6B	Keratin 6B	-4.91	9.95E-08
	KRT14	Keratin 14	-4.64	3.26E-06			KRT6C	Keratin 6C	-4.25	5.86E-09
	KRT6C	Keratin 6C	-4.50	7.15E-17			SPRR18	Small Proline Rich Protein 18	-4.04	4.63E-07
	KRT7	Keratin 7	-4.42	2.62E-11			KRT17	Keratin 17	-4.00	6.38E-06
	KRT16	Keratin 16	-4.38	2.24E-06			LY6D	Lymphocyte Antigen 6 Family Member D	-3.81	1.66E-06
	DSP	Desmoplakin	-4.25	8.73E-16			PI3	Peptidase Inhibitor 3	-3.68	6.74E-10
	KRT5	Keratin 5	-4.15	7.12E-05						
	Cluster 7	Up-regulated genes						Cluster 12	Up-regulated genes	
MMP3		Matrix Metalloproteinase 3	5.59	2.08E-11		-	-		-	-
MMP1		Matrix Metalloproteinase 1	5.23	2.40E-13		Down-regulated genes				
CHI3L1		Chitinase-3-like protein 1	4.93	6.50E-12		PRSS12	Serine Protease 12		-3.54	3.98E-05
G0S2		G0/G1 Switch 2	4.03	8.63E-07		FABP4	Fatty Acid Binding Protein 4		-3.3	4.38E-08
CHI3L2		Chitinase-3-like protein 2	3.51	2.13E-05		PODXL	Podocalyxin Like		-3.13	0.00181
CXCL8		C-X-C Motif Chemokine Ligand 8	3.49	0.000129		TIMP3	Tissue Inhibitor Of Metalloproteinases 3		-3.11	2.57E-06
DERL3		Der1-Like Domain Family, Member 3	3.47	1.18E-12		APOD	Apolipoprotein D		-3.05	1.49E-06
CXCL6		C-X-C Motif Chemokine Ligand 6	3.29	0.0019		ECSCR	Endothelial Cell Surface Expressed Chemotaxis And Apopt		-3.00	2.06E-09
TDO2		Tryptophan 2,3-Dioxygenase	3.24	6.21E-05		SOX13	SRY-Box Transcription Factor 13		-2.89	3.13E-05
PIM2		Serine/Threonine-Protein Kinase Pim-2	3.22	1.25E-12		PCDH18	Protocadherin 18		-2.71	3.33E-05
Down-regulated genes					COMP	Cartilage Oligomeric Matrix Protein	-2.67		0.0481	
COMP		Cartilage Oligomeric Matrix Protein	-4.75	1.87E-35		CD200	CD200 Molecule		-2.63	1.38E-08
APOD		Apolipoprotein D	-4.32	1.15E-38						
PRELP		Proline & Arginine Rich End Leucine Rich Repeat Protein	-4.28	7.11E-36						
ITGBL1		Integrin Subunit Beta Like 1	-3.91	1.56E-37						
OMD		Osteomodulin	-3.69	6.77E-28						
COL14A1		Collagen Type XIV Alpha 1 Chain	-3.56	3.04E-18						
THSD4		Thrombospondin Type 1 Domain Containing 4	-3.54	1.31E-25						
KRT1		Keratin 1	-3.27	3.86E-10						
ABI3BP		ABI Family Member 3 Binding Protein	-3.25	1.18E-24						
CFD		Complement Factor D	-3.23	1.22E-13						

Premio Goldman Sachs 2024

Table 2 - The 20 most up- or down-regulated genes identified by RNA-sequencing in peri-implantitis versus reference implant specimens

Ensemble ID	Gene symbol	Gene name	Log2 fold change	Adjusted p-value
Up-regulated genes				
ENSG00000163735	CXCL5	C-X-C motif chemokine ligand 5	3.73	3.55E-12
ENSG00000095059	DHPS	deoxyhypusine synthase	3.05	3.17E-08
ENSG00000095059	TMCC2	transmembrane and coiled-coil domain family 2	1.14	1.75E-06
ENSG00000163421	PROK2	prokineticin 2	2.39	1.75E-06
ENSG00000261594	TPBGL	trophoblast glycoprotein like	1.83	1.75E-06
ENSG00000140451	PIF1	PIF1 5'-to-3' DNA helicase	2.15	5.70E-06
ENSG00000119535	CSF3R	colony stimulating factor 3 receptor	2.11	1.33E-05
ENSG00000149968	MMP3	matrix metalloproteinase 3	2.32	1.33E-05
ENSG00000108342	CSF3	colony stimulating factor 3	2.48	1.33E-05
ENSG00000108342	ZSWIM1	zinc finger SWIM-type containing 1	1.78	1.90E-05
Down-regulated genes				
ENSG00000123975	CKS2	CDC28 protein kinase regulatory subunit 2	-0.96	6.04E-05
ENSG00000123975	DLK2	delta like non-canonical Notch ligand 2	-1.68	8.66E-05
ENSG00000173338	KCNK7	potassium two pore domain channel subfamily	-1.97	8.66E-05
ENSG00000173338	UBFD1	ubiquitin family domain containing 1	-0.40	0.00013626
ENSG00000126233	SLURP1	secreted LY6/PLAUR domain containing 1	-1.45	0.00015198
ENSG00000163331	DAPL1	death associated protein like 1	-1.84	0.00016741
ENSG00000167900	TK1	thymidine kinase 1	-1.16	0.00018242
ENSG00000065621	GSTO2	glutathione S-transferase omega 2	-1.54	0.00019747
ENSG00000186832	KRT16	keratin 16	-1.83	0.00021115
ENSG00000178934	LGALS7	galectin 7	-1.77	0.00029184

Appendix – Supplementary material

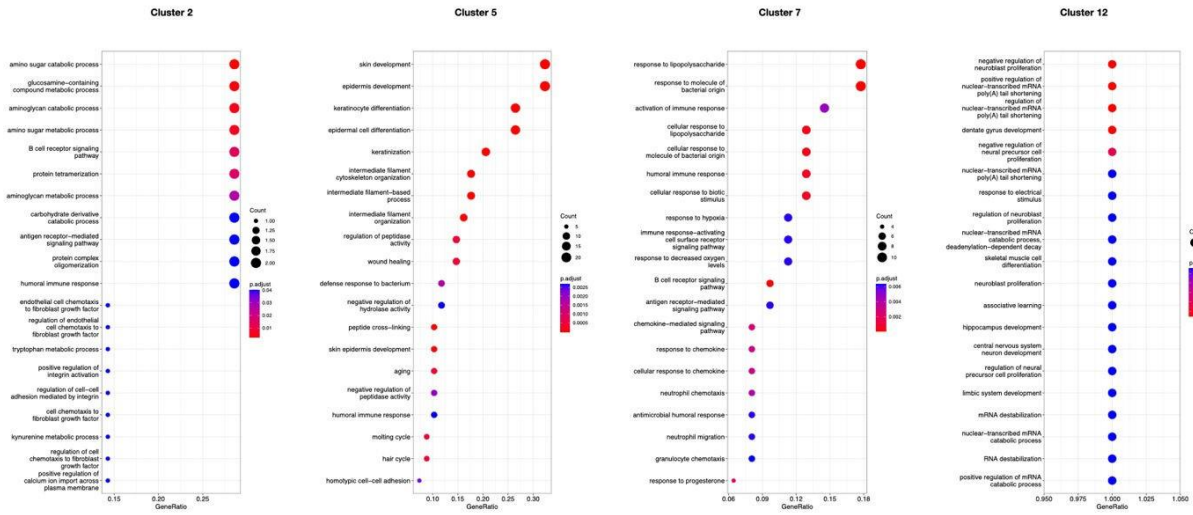
Supplementary Table 1. Patient characteristics

Spatial transcriptomics (N=2)		
	<i>mean / %</i>	<i>sd</i>
Age	77.0	7.07
Gender		
	<i>Female</i>	100%
Smoking		
	<i>No</i>	100%
Diabetes		
	<i>Yes</i>	50%
RNA-sequencing (N=10)		
	<i>mean / %</i>	<i>sd</i>
Age	73.8	11.97
Gender		
	<i>Female</i>	100%
Smoking		
	<i>No</i>	90%
Diabetes		
	<i>Yes</i>	20%

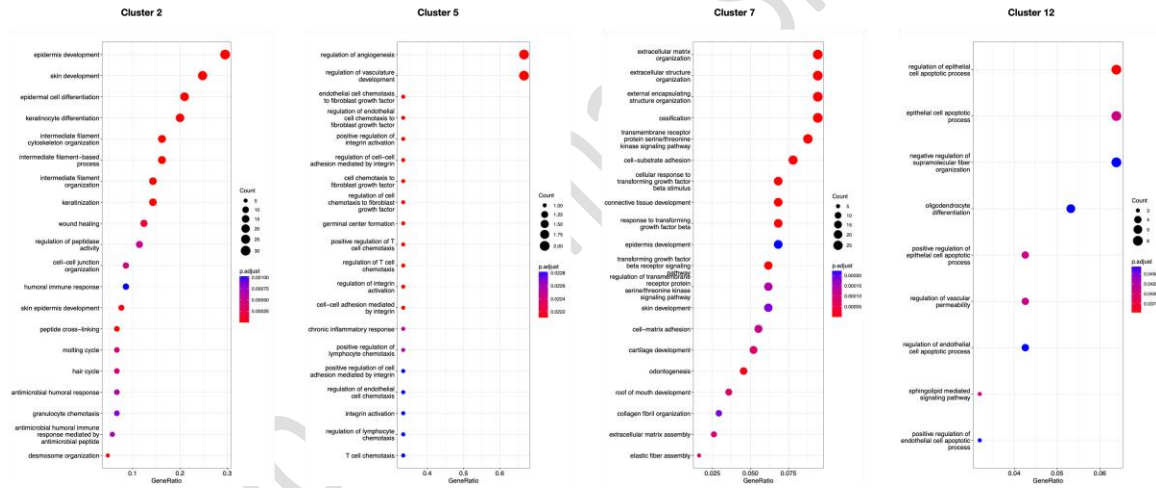
Supplementary table 2. Clinical measurements

	Peri-implantitis		Reference implant	
	<i>mean / %</i>	<i>sd</i>	<i>mean / %</i>	<i>sd</i>
Spatial transcriptomics	n=2		n=2	
Probing pocket depth (mm)	8.0	0.0	4.0	1.41
Radiographic bone level (mm)	4.6	1.46	0.9	0.28
Bleeding on probing (%)	100%		50%	
Suppuration on probing (%)	50%		0%	
RNA-sequencing	n=10		n=10	
Probing pocket depth (mm)	7.6	0.70	3.7	0.82
Radiographic bone level (mm)	4.4	0.81	1.3	0.83
Bleeding on probing (%)	100%		50%	
Suppuration on probing (%)	50%		0%	

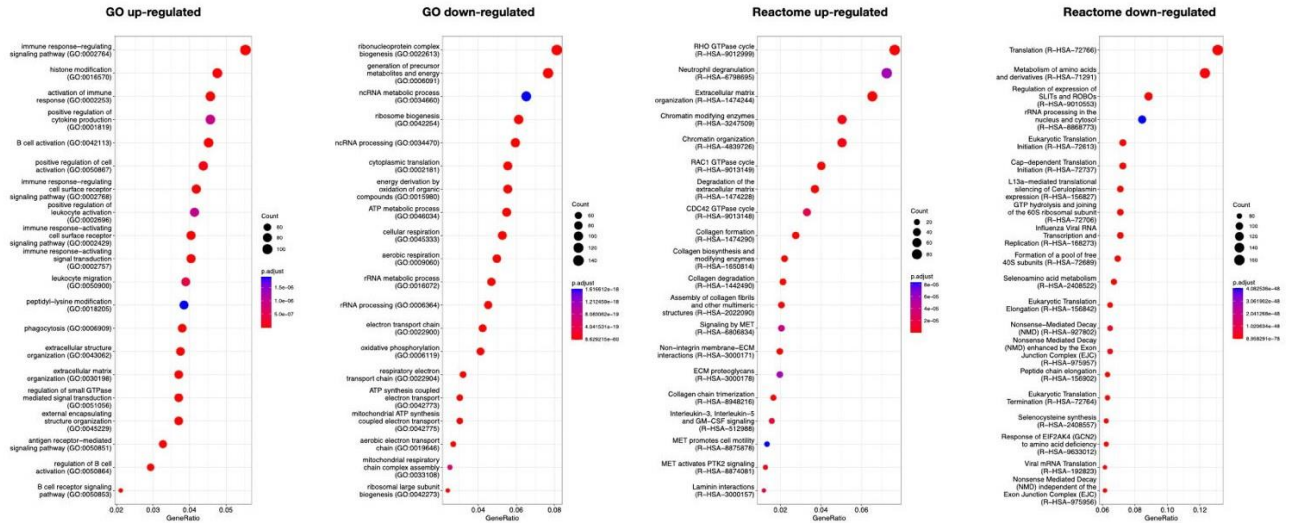
a. GO up-regulated



b. GO down-regulated



Supplementary Figure 1. Gene Ontology enrichment analysis from *spa/al* transcriptomic data. a) Up-regulation. b) Down-regulation.



Supplementary Figure 2. Gene Ontology and Reactome enrichment analyses from RNA-sequencing data.